Orientational order parameters in liquid crystals: A comparative study of x-ray diffraction and polarized Raman spectroscopy results

Alberto Sanchez-Castillo,[1] Mikhail A. Osipov,[2] and Frank Giesselmann[1]
[1]*Institut für Physikalische Chemie, Universität Stuttgart, Pfaffenwaldring 55, 70569 Stuttgart, Germany*
[2]*Department of Mathematics, University of Strathclyde, Glasgow, United Kingdom*
(Received 30 June 2009; published 23 February 2010)

The orientational order parameters $\langle P_2\rangle$ and $\langle P_4\rangle$ in the nematic liquid crystal 4-pentyl-4'-cyanobipheny (5CB) have been determined by means of the two completely different techniques: polarized Raman spectroscopy and x-ray scattering. In particular, the values of $\langle P_2\rangle$ and $\langle P_4\rangle$ obtained using two different Raman methods, proposed by Jen *et al.* [J. Chem. Phys **66**, 4635 (1977)] and Jones *et al.* [J. Mol. Struct. **708**, 145 (2004)], respectively, are compared with the results of x-ray measurements. A good agreement between the experimental values of $\langle P_2\rangle$ and $\langle P_4\rangle$ and the results of the Humphries-James-Luckhurst mean field theory has been found whenever they were determined using either x-ray measurement or following the Jen *et al.* method. In addition, a study of the influence of the intensity of the exiting laser source on the apparent values of the order parameters has been performed. Therefore, it was found that the discrepancies of the value of $\langle P_4\rangle$ determined following Jen *et al.* and Jones *et al.* could be determined by nonlinear effects.

DOI: 10.1103/PhysRevE.81.021707 PACS number(s): 61.30.Cz, 78.30.Jw, 64.70.M−

I. INTRODUCTION

The orientational order parameters of various liquid crystal phases have attracted a significant attention during the last decades since these quantities characterize the degree of intrinsic long range orientational order in liquid crystals. In thermotropic liquid crystals, the molecules are normally assumed to possess the effective cylindrical symmetry [1], i.e., the short molecular axes are assumed to be distributed randomly about the long molecular axes. The average orientation of the molecular long axes is usually defined by a macroscopic symmetry axis known as the director **n**. Since the molecules are constantly in thermal motion, the long axis of any molecule at any moment makes some angle β with respect to **n**. The orientational order of such molecules in a liquid crystal phase is then described by an orientational distribution function $f(\beta)$ [2].

Although $f(\beta)$ can completely characterize the intrinsic molecular state of the system, only few techniques are capable of measuring the total distribution function $f(\beta)$. Neutron and x-ray diffraction studies have been undertaken for many liquid crystalline materials [3,4]. These techniques can, in principle, be used to measure the distribution function $f(\beta)$ but the main disadvantage is that accurate measurements of intensity are required. In fact, most of the experimental techniques cannot be used to measure the total distribution function, but can be used to measure a truncated one.

In the case of uniaxial nematic liquid crystals, composed of uniaxial molecules, the orientational distribution function depends on the Euler angle β only and can be expanded in terms of the Legendre polynomials $\langle P_L(\cos\beta)\rangle$ [5]. In many cases, however, it is sufficient to use a truncated expansion which is consistent with the standard phenomenological description in terms of few order parameters. Actually, the first two nontrivial orientational order parameters, $\langle P_2(\cos\beta)\rangle$, and $\langle P_4(\cos\beta)\rangle$, are of particular interest since they can be measured experimentally. Here, the angular brackets $\langle\ldots\rangle$ denote the statistical average.

The order parameter $\langle P_2\rangle$ can be determined experimentally by many methods such as nuclear magnetic resonance (NMR), dielectric permittivity, IR absorption, magnetic susceptibilities, refractive index measurements, and electronic and vibrational spectroscopy [6–9]. In contrast, the parameter $\langle P_4\rangle$ is particularly difficult to measure. The x-ray and neutron diffraction, polarized fluorescence, two photon dichroism, electron paramagnetic resonance (EPR), and polarized Raman spectroscopy (PRS) are among the experimental methods that can in principle be used to measure $\langle P_4\rangle$. However, only few of them have been implemented in practice with a degree of success [3,5,10–13].

In their pioneering work, Jen *et al.* laid the foundations to determine simultaneously $\langle P_2\rangle$ and $\langle P_4\rangle$ using PRS in a backscattering configuration [5]. In this technique, measurements of vibrational Raman depolarization ratios in different orthogonal linear polarization conditions are used to find the order parameters $\langle P_2\rangle$ and $\langle P_4\rangle$ in liquid crystals. The values of $\langle P_2\rangle$ obtained using this method are in agreement with theory and with previous results derived using several other techniques [3–18]. At the same time, the values of $\langle P_4\rangle$ are in disagreement with those results even taking into account experimental error. In fact, the order parameter $\langle P_4\rangle$ was unexpectedly found to be negative for many materials [5,14–18]. One notes that such negative values cannot be found in simple molecular field theories such as those proposed by Maier-Saupe (MS) [1] or Humphries-James-Luckhurst (HJL) [19]. Several attempts have been made in order to explain these results [17] but no convincing argument has been found. Other ideas, regarding internal field correction, have also been suggested [20]. Although these corrections improved the results of $\langle P_4\rangle$, they were not enough to fit the values in any of the molecular field theories. Moreover, the values for $\langle P_4\rangle$ were still lower than those predicted by the Maier-Saupe theory.

In recent years, Jones *et al.* extended the experimental work done by Jen *et al.* and developed an advanced method to determine both $\langle P_2 \rangle$ and $\langle P_4 \rangle$ by the same fitting procedure [21]. This method is based on the measurements of detailed intensity profiles of the scattered Raman signal as a function of the angle between the director and the laboratory frame using two different polarization conditions. The order parameters and the differential polarizability ratio r can then be obtained from a simultaneous fitting procedure of such intensities profiles, I_{zz} and I_{yz}. The main advantage of this method is that only one planar-aligned sample is required unlike the method by Jen *et al.*, where three different alignment geometries have to be used. With this advanced method Jones *et al.* have been able to obtain the value of the order parameter $\langle P_4 \rangle$ for the nematic material E7 (at an isolated temperature inside the nematic phase), which is much closer to the results of the molecular theories.

Finally, the "mystery" related to abnormally low or even negative values of the order parameter $\langle P_4 \rangle$ has recently been resolved by Southern and Gleeson [22] who have used the method of Jones *et al.* to study the temperature variation in both $\langle P_2 \rangle$ and $\langle P_4 \rangle$ throughout the whole of the nematic phase in the material 4-*n*-octyl-4'-cyanobipheny (8CB). As shown in [22], the value of $\langle P_4 \rangle$ is particularly sensitive to the value of the differential polarizability r which is allowed to vary as a fitting parameter in the method of Jones *et al.* It has been found that r varies significantly within the nematic range of 8CB and is different from its value in the isotropic phase. Taking this into account, a very good agreement between the experimental values of $\langle P_4 \rangle$ and the results of the HJL theory has been obtained. In contrast, if r is assumed to be constant and to be the same in the nematic and the isotropic phases, the apparent values of $\langle P_4 \rangle$ are decreased approximately by a factor of two. Recently, the same method has also been used to determine the order parameters of the biaxial nematic phase [23].

As mentioned above, the x-ray technique is another conventional method to determine the values of $\langle P_2 \rangle$ and $\langle P_4 \rangle$ [3,4,24,25]. At the same time, x-ray and Raman experiments probe features of the sample in two different ways. Indeed, the x-ray diffraction pattern originates from the interaction between the x-ray beam and the electron density distribution inside the sample [26]. On the other hand, the scattered Raman signal is the result of the interaction between the incoming light and the molecular polarizability [27]. Despite this difference, both methods should yield, in principle, similar information about the orientational order parameters. However, as far as we know, the two techniques have never been used simultaneously to determine $\langle P_2 \rangle$ and $\langle P_4 \rangle$ for the same nematic material in order to compare the results.

In this paper, we use both polarized Raman spectroscopy and x-ray scattering to determine the order parameters $\langle P_2 \rangle$ and $\langle P_4 \rangle$ of the nematic liquid crystal 5CB by two independent techniques. Moreover, we use both methods, proposed by Jen *et al.* and Jones *et al.*, respectively, to extract the values of $\langle P_2 \rangle$ and $\langle P_4 \rangle$ from Raman data in different geometries, and compare the results. We also study of the influence of the intensity of the exiting laser source on the apparent values of the order parameters.

The paper is arranged as follows: First, the main characteristics of the Raman tensor are briefly discussed. Then, Secs. III and IV cover the fundamentals points of the Raman methods, developed by Jen *et al.* and Jones *et al.*, respectively, used in this work to determine the order parameters. Section V explains the basic ideas to obtain $\langle P_2 \rangle$ and $\langle P_4 \rangle$ from the x-ray measurements. The experimental details are described in Sec. VI. Thereafter, Sec. VII gives a quite detailed discussion of the order parameters obtained using the methods of Secs. III–V. Finally, the conclusion of the work are presented in Sec. VIII

II. RAMAN TENSOR

When linearly polarized light interacts with a molecule, the electron cloud is distorted by an amount that depends on its ability to polarize, and this effect is specified by the molecular second rank polarizability tensor α_{ij}. The induced distortion can be described as an induced molecular dipole which has a certain orientation in the molecular frame x, y, and z. The results of the interaction between light and the medium gives rise to the Rayleigh and Raman scattering [27].

In particular, Raman scattering is an inelastic scattering process since the Raman signal is shifted in wavelength from the incident light. The intensity I of the Raman signal is proportional to the square of the polarizability derivative with respect to the distortion coordinate Q_k, $I \propto (\partial_{Qk} \alpha_{ij})^2 \equiv (\alpha'_{ij})^2$, and the absolute values for α'_{ij} depend upon the choice of coordinates. For convenience, a polarizability ellipsoid fixed in the molecular frame is usually selected thus defining the principal axes frame x',y',z'.

As a matter of fact, there is always a frame where the Raman tensor can be reduced to a diagonal form for every particular vibration k as follows:

$$\alpha'_{ij} = \begin{bmatrix} \alpha'_{x'x'} & 0 & 0 \\ 0 & \alpha'_{y'y'} & 0 \\ 0 & 0 & \alpha'_{z'z'} \end{bmatrix}. \tag{1}$$

However, a coordinate transformation between the molecular and the laboratory frame is still required since all the physical quantities are measured in the latter frame. Consider the Euler angles (ϕ, β, γ) which specify the rotations transforming the molecular frame $x'y'z'$ into the laboratory one xyz. Then, such a transformation can be described in terms of the director cosines as [27]

$$\alpha_{xy} = \sum_{x'y'} \alpha_{x'y'} \cos(xx') \cos(yy'). \tag{2}$$

For particular successive rotation matrices with rotation angles ϕ, β, and γ, respectively, the following expression can be derived:

$$\begin{array}{c|ccc} & x & y & z \\ x' & \cos\phi\cos\beta\cos\gamma-\sin\phi\sin\gamma & \sin\phi\cos\beta\cos\gamma+\cos\phi\sin\gamma & -\sin\beta\cos\gamma \\ y' & -\cos\phi\cos\beta\sin\gamma-\sin\phi\cos\gamma & -\sin\phi\cos\beta\sin\gamma+\cos\phi\cos\gamma & \sin\beta\cos\gamma \\ z' & \cos\phi\sin\beta & \sin\phi\sin\beta & \cos\beta \end{array}. \tag{3}$$

III. JEN *et al.* METHOD

The extensive work made by Jen and co-workers to use Raman scattering in nematic liquid crystals gave a reasonably good and really detailed description of the problem [5]. In this approach, the measured polarization ratios can be related to the averages of various components of the polarizability tensor in the molecular frame. Experimentally, a set of aligned systems is required (i.e., planar and homeotropic cells, see Fig. 1) and only four independent statistical averages of polarizability components $\langle \alpha_{ij}, \alpha_{ij} \rangle$, (under the correct transformation of coordinates) are needed to define the depolarization ratios as

$$R_1 = C_n \frac{\langle \alpha_{yz}^2 \rangle}{\langle \alpha_{zz}^2 \rangle}; R_2 = \frac{\langle \alpha_{zy}^2 \rangle}{C_n \langle \alpha_{yy}^2 \rangle}; R_3 = \frac{\langle \alpha_{yx}^2 \rangle}{\langle \alpha_{xx}^2 \rangle}. \tag{4}$$

Where, in general;

$$C_n = \left(\frac{n_g + n_e}{n_g + n_o} \right), \tag{5}$$

$$A^{-2}\langle \alpha_{xx}^2 \rangle = \frac{1}{9} + \frac{3}{16}B + \frac{1}{18}D + \frac{11}{288}D^2 + \left(\frac{1}{8}B - \frac{1}{6}D - \frac{5}{48}D^2 \right) \times \langle \cos^2\beta \rangle + \left(\frac{3}{16}B + \frac{2}{32}D^2 \right) \langle \cos^4\beta \rangle, \tag{6}$$

$$A^{-2}\langle \alpha_{yx}^2 \rangle = \frac{1}{16}B + \frac{1}{32}D^2 + \left(\frac{3}{8}B - \frac{1}{16}D^2 \right) \langle \cos^2\beta \rangle + \left(\frac{1}{16}B + \frac{1}{32}D^2 \right) \langle \cos^4\beta \rangle, \tag{7}$$

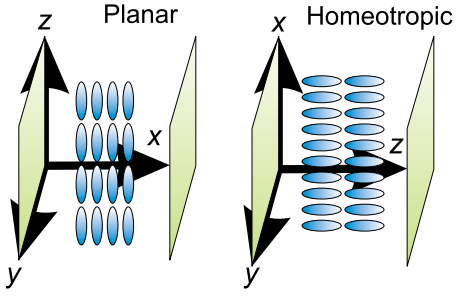

FIG. 1. (Color online) Experimental Raman geometries used to measure the depolarization ratio R_1, R_2, and R_3 in liquid crystal according to Jen *et al.* The planar geometry is also used to measure the intensity profiles I_{zz} and I_{yz} following the method of Jones *et al.* when the sample is rotated. The x, y, z axis represent the laboratory frame.

$$A^{-2}\langle \alpha_{yx}^2 \rangle = \frac{1}{4}B + \left(\frac{1}{8}D^2 \right) \langle \cos^2\beta \rangle - \left(\frac{1}{4}B + \frac{1}{8}D^2 \right) \langle \cos^4\beta \rangle, \tag{8}$$

$$A^{-2}\langle \alpha_{zz}^2 \rangle = \frac{1}{9} + \frac{1}{2}B - \frac{1}{9}D + \frac{1}{36}D^2 - \left(B - \frac{1}{3}D - \frac{1}{6}D^2 \right) \langle \cos^2\beta \rangle + \left(\frac{1}{2}B + \frac{1}{4}D^2 \right) \langle \cos^4\beta \rangle. \tag{9}$$

With $A = 1 + r + s$; $B = \frac{(r-s)^2}{4A^2}$; $D = \frac{2-r-s}{A}$.

Here, C_n is a correction factor, which accounts for a difference in the reflection and refraction at the liquid crystal-glass interface. n_o, n_e, and n_g are the ordinary, extraordinary, and glass slides refractive indices, respectively. In addition, the subscripts ij, with $i, j = x, y, z$, denote that the sample is placed between cross ($i \neq j$) or parallel ($i = j$) polarizers.

Furthermore, $r = s$ only when the particular vibration under study has the uniaxial symmetry in the local frame. Therefore, under this condition, the differential polarizability ratio $r = \alpha'_{xx} / \alpha'_{zz}$ can be evaluated using the following equation:

$$R_{iso} = \frac{(1-r)^2}{(3 + 4r + 8r^2)}. \tag{10}$$

Where R_{iso} is the depolarization ratio determined in the isotropic phase of the liquid crystal. We consider the case of uniaxial symmetry throughout this paper.

IV. JONES *et al.* METHOD

A similar theoretical analysis, with the same basic idea of Jen and co-workers, was developed by Jones *et al.* [21]. In order to determine the orientational order parameters using polarized Raman spectroscopy. One notes that the method described by Jones is more general since it takes into account the whole polarization angle dependence of the Raman signal instead of only two possible configurations as proposed by Jen *et al.* [5]. In general, the main idea here is to consider the classical oscillating dipole in the molecular frame, which makes an angle θ with respect to the polarization direction of the incoming beam, and to link it to the laboratory frame using the correct transformation of coordinates.

Furthermore, the oscillating dipole described as $\boldsymbol{\mu} = \alpha_{ij}\mathbf{E}$, where E is the local electric field and α_{ij} is the molecular

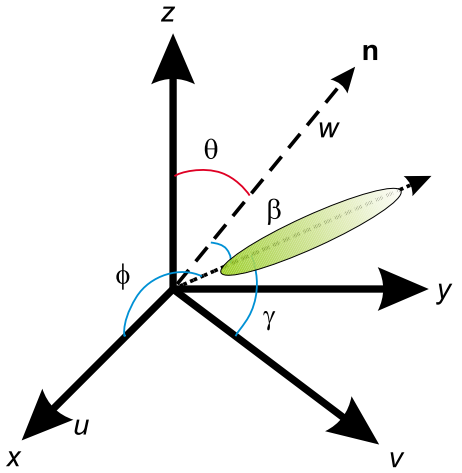

FIG. 2. (Color online) Relationship between Cartesian coordinates in the molecular (u,v,w) and the laboratory (x,y,z) frames via the Euler angles (ϕ,β,γ). The angle between the polarization vector of the incoming beam and the director **n** is θ.

polarizability, is a quantity which fluctuates together with the molecular long axis about the director (see Fig. 2). Thus, it is necessary to takes into account the statistical distribution of molecular long axes in the system described by the orientational distribution function (ODF) $f(\beta)$. Similar to the Jen's method, the nematic cell is placed between crossed and parallel polarizers but, in addition, the sample is also rotated in the plane perpendicular to the propagation direction of the incoming beam. Consequently, the detected intensity profile can be expressed in terms of the components of the polarizability in the laboratory frame, which depend on the Euler angles (ϕ,β,γ), the angle θ, and the distribution function using the following equation:

$$I_{ij}(\theta) = I_0 \int_{\alpha,\beta,\gamma} f(\beta)[\alpha'_{ij}(\phi,\beta,\gamma,\theta)]^2 d\beta. \tag{11}$$

I_0 is the intensity of the incoming beam and ij are the subscripts for the polarization direction of the analyzer and polarizer after (j) and before (i) the sample. Based on this idea, Jones *et al.* derived the follow pair of equations for a planar sample in which the director **n** makes an angle θ with the polarization direction of the incoming beam. Apart from that, the Raman signal is analyzed with a polarizer oriented parallel or perpendicular to the polarization state of the incoming beam. Consequently, the intensity profile is characterized by the following pair of expressions [21]:

$$\frac{I_{zz}(\theta)}{I_{zz}(0)} = \frac{a + b\langle P_2\rangle + 3c\langle P_4\rangle - 3b\langle P_2\rangle\cos^2\theta - 30c\langle P_4\rangle\cos^2\theta + 35c\langle P_4\rangle\cos^4\theta}{a - 2b\langle P_2\rangle + 8c\langle P_4\rangle}, \tag{12}$$

$$\frac{I_{yz}(\theta)}{I_{zz}(0)} = \frac{d - e\langle P_2\rangle - 4c\langle P_4\rangle + 35c\langle P_4\rangle\cos^2\theta\sin^2\theta}{a - 2b\langle P_2\rangle + 8c\langle P_4\rangle}. \tag{13}$$

Where $a=(8r^2+4r+3)/15$; $b=(8r^2-2r-6)$; $c=(r-1)^2/35$; $d=(r-1)^2/15$; $e=-(r-1)^2/21$. $\langle P_2\rangle=\langle 3\cos^2\beta-1\rangle/2$ and $\langle P_4\rangle=\langle 35\cos^4\beta-30\cos^2\beta+3\rangle/2$ are the orientational order parameters. In this way, $\langle P_2\rangle$, $\langle P_4\rangle$, and r can be calculated using a fitting procedure of such intensity profiles.

V. X-RAY SCATTERING THEORY

In uniaxially aligned liquid crystal samples, after the interaction with the x-ray beam, the order parameters as well as the ODF are experimentally available from the intensity profile $I(\chi)$ around the wide-angle arc of diffuse x-ray scattering [24], Fig. 3. The relationship between the ODF and the intensity profile $I(\chi)$ was first established by Leadbetter and Norris [3] who derived an expression which allows calculating $I(\chi)$ directly from $f(\beta)$ as follows:

$$I(\chi) = \int_{\beta=\chi}^{\pi/2} \frac{f(\beta)\sin\beta\sec^2\chi}{\sqrt{\tan^2\beta - \tan^2\chi}} d\beta. \tag{14}$$

In order to extract $f(\beta)$ from the experimental $I(\chi)$ profile, a difficult numerical inversion of Eq. (14) is needed. However, Davidson *et al.* [28] developed a simpler method to evaluate $f(\beta)$. The basic idea behind this method is to expand the ODF in terms of $\cos^{2n}\beta$ functions instead of Legendre polynomials as

$$f(\beta) = \sum_{n=0}^{\infty} f_{2n}\cos^{2n}\beta. \tag{15}$$

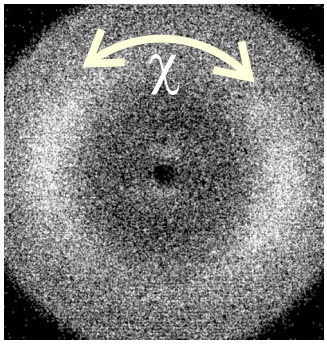

FIG. 3. (Color online) Diffracted pattern generated after the x-ray scattering in the nematic phase of 5CB measured in this experiment at 25 °C. The wide-angle arc χ is shown.

As shown by Davidson *et al.*, the resulting intensity profile derived from Eq. (14) is also expressed as a series of $\cos^{2n}$ functions involving the same f_{2n}. Thus, the scattering profile $I(\chi)$ is related to the coefficients of the ODF in a simple form according to the following expression:

$$I(\chi) = \sum_{n=0}^{\infty} f_{2n} \frac{2^n n!}{(2n+1)!!} \cos^{2n} \chi. \tag{16}$$

Hence, the function $f(\beta)$ can directly be calculated by inserting the fitted f_{2n} into Eq. (15). As a result, the orientational order parameters are calculated as moments of the ODF as follows:

$$\langle P_{2n} \rangle = \frac{\int_0^{\pi/2} P_{2n} f(\beta) \sin(\beta) d\beta}{\int_0^{\pi/2} f(\beta) \sin(\beta) d\beta}; \quad n = 1,2. \tag{17}$$

VI. EXPERIMENT

One of the most popular nematic liquid crystal materials, 4-pentyl-4-cyanobiphenyl (5CB), has been used in our experiment. This material has been selected because it has already been employed in previous studies where $\langle P_2 \rangle$ and $\langle P_4 \rangle$ has been determined by the Raman technique [14]. This serves as a reference to verify our results. Recently, a similar material 8CB has also been studied using the Raman technique [22].

Several liquid crystal samples for Raman studies were prepared using fused silica plates rubbed with polymid. Two nematic cells were prepared each with planar alignment on both plates and with 25 or 12 μm spacers, respectively. Another sample was homeotropically aligned and separated by 20 μm spacers. In the x-ray case, the 5CB was filled into a Mark capillary tube with 0.7 mm diameter.

A Horiba Jobin Yvon confocal Raman spectrometer HR-800 equipped with a 614 nm He-Ne laser operating at 20 mW and a CCD camera has been used to measure the backscattered Raman signal of the 5CB, Fig. 4. The laser is linearly polarized and neutral density filters with optical density of 0.3, 0.6 1, 2, 3 are selected to attenuate its optical power. In order to get a good signal to noise ratio of the Raman spectra, the dimension of the confocal hole and the entrance slit were fixed for all measurements at 300 and 200 μm, respectively. The objective of the microscope was a 50x with a N.A of 0.45 which is able to focus on the sample in a spot around 8 μm. In addition, the linear incoming polarized light is rotated by introducing a $\lambda/2$ plate in front of the laser beam. An analyzer and a depolarizer are fixed and placed just before the slit entrance. This configuration allows us to reduce the polarization dependence effect of the detection system. When the linear polarization state of the incoming beam and that of the outcoming beam after the analyzer are parallel we denoted this as the zz configuration. In contrast, when the above mentioned linear polarization states are orthogonal, we denoted this as the yz configuration. Additionally, the sample is placed inside a rotatable hot stage (Linkam) in order to study the angle and temperature dependence of the molecular polarizability with respect to the polarization of the incident beam, see Fig. 4.

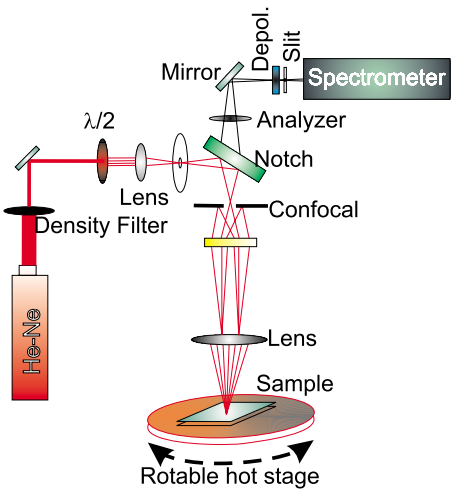

FIG. 4. (Color online) Experimental Raman setup used to measure the order parameters. The depolarizer and the analyzer are in a fixed position as well as the dimension of the slit and the confocal hole. The depolarization ratios and the intensity profiles I_{zz} and I_{yz} can be measured changing either the $\lambda/2$ plate or rotating the sample.

The spectra were taken every 10° until an entire 360° rotation of the hot stage was accomplished. The temperature and rotation accuracies are ±0.1 °C and 2°, respectively.

As a matter of fact, it is well known that the 1606 cm^{-1} Raman band in 5CB is originated from the phenyl rings stretching mode, which is uniaxial and strongly polarized along the molecular axis [29]. This vibration was studied throughout the experiment. Finally, the Raman spectra were recorded and analyzed with LABSPEC software in a range of 900–2300 cm^{-1} in order to be able to remove the background of the whole spectra instead of only that of the particular peak. The next step is fitting the Raman peak at 1606 cm^{-1} to a Lorentzian function in order to determine the area under the peak. Thus, this integrated intensity was used to determine the average $\langle \alpha_{ij}, \alpha_{ij} \rangle$ at certain temperatures, polarization conditions and relative orientations of the sample.

On the other hand, x-ray scattering measurements were carried out with a Bruker NanoStar diffractometer using Ni-filtered Cu K_α radiation. The capillary sample was mounted in a temperature controlled brass block and kept in a 1 T horizontal magnetic field. The temperature controller system has a resolution of ±0.1 °C. A two-dimensional diffraction pattern was recorded using a HiStar area detector. In addition, small-angle x-ray scattering (SAXS) software from Bruker Co. was used to extract the intensity profile of the wide-angle diffraction pattern.

VII. RESULTS AND DISCUSSION

A. Order parameters $\langle P_2 \rangle$ and $\langle P_4 \rangle$ determined by PRS, Jen *et al.* method

The results obtained from the PRS experiments are presented as follows. At the first stage, the depolarization ratios

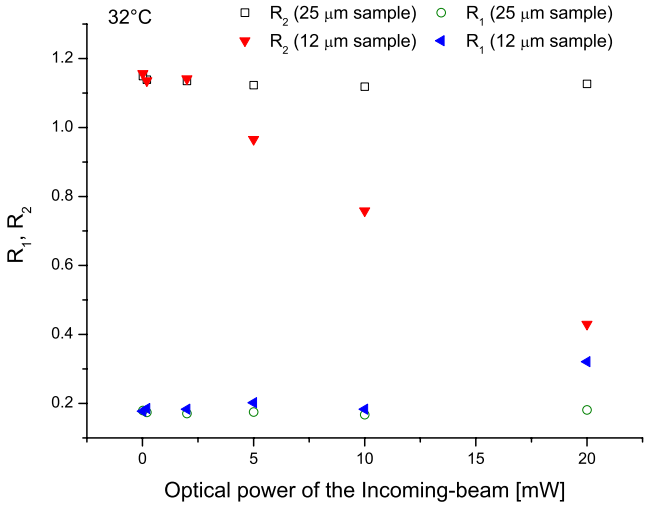

FIG. 5. (Color online) Depolarization ratios R_1 and R_2 for samples with thickness of 25 and 12 μm at 32 °C. The values of R_1 and R_2 for the 12 μm sample show a strong dependence on the intensity of the illuminating beam. In contrast, for the 25 μm sample, the values of R_1 and R_2 are practically constant.

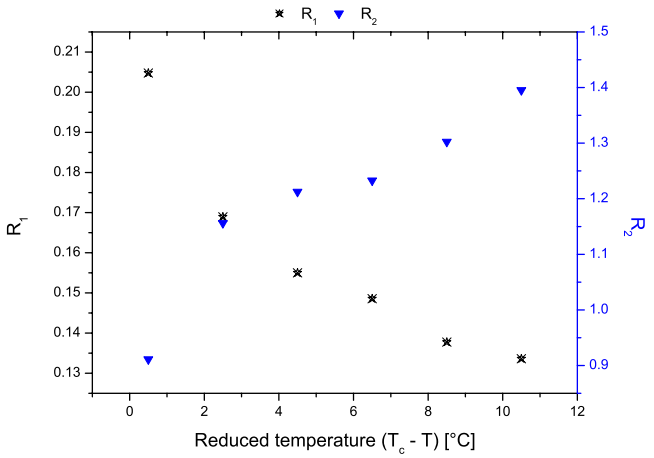

FIG. 6. (Color online) Depolarization ratios R_1 and R_2 determined in the 12 μm sample using the optical power of 2 mW. The order parameters were evaluated using these values of R_1 and R_2.

for planar and homeotropically aligned samples with thickness of 12, 25, and 20 μm, respectively, were determined following the method described by Jen *et al.* In accordance with this method, the extrapolation to zero thickness has been a routinely procedure to evaluate the depolarization ratio R_1 and R_2 of a liquid crystal substance in order to avoid multiple scattering effects [5,14–18]. A detailed comparison of the dependence on thickness of these depolarization ratios for various liquid crystals compounds, showing different degrees of dielectric and optic anisotropy, is given in ref [17]. Basically, a linear behavior of R_1 and R_2 with cell thickness was found for liquid crystal cells with a thickness in a typical range of around 12–80 μm.

On the other hand, the use of a focused laser beam on the sample requires a previous analysis of the depolarization ratios R_1 and R_2 as a function of the intensity of the incoming laser as well. This dependence is shown in Fig. 5 for a particular temperature and is expressed in terms of the optical power of the laser beam before it is focused on the sample. This behavior is surprising and has not been reported so far. It is found that the effective values of R_1 and R_2 do not depend significantly on the intensity of the incoming beam if the 25 μm sample is used. In contrast, the 12 μm sample shows a strong dependence on the optical power of the laser, and thus one must be careful when the depolarization ratios are measured in this sample in order to find the correct values of R_1 and R_2.

In addition, Fig. 5 indicates that the depolarization ratios for 5CB (R_1 and R_2) have practically the same value in samples with different thickness when the intensity of the laser beam is less or equal to 2 mW. Therefore, there is no need to extrapolate the experimental data to zero thickness when the adequate intensity of the incoming beam is selected and the average values of R_1 and R_2, over several measurements in both the 12 and the 25 μm thickness samples, are taken.

The order parameter $\langle P_2 \rangle$ for a particular nematic liquid crystal has been determined from birefringence measurements in Ref. [30]. That work showed that $\langle P_2 \rangle$ is enhanced in cells as thin as 2 μm due to the walls effects of the cell. Therefore, it is reasonable to exclude this wall effect in our 12 μm cell.

Under these conditions, the experimental values of R_1 and R_2 with respect to temperature are shown in Fig. 6. In order to determine R_1 and R_2, the refractive indices n_o and n_e were taken from reference [31] and the refractive index of the glass was taken as $n_g = 1.515$.

The depolarization ratio of 5CB in the isotropic phase, for the phenyl stretching mode, was determined experimentally at 38 °C as $R_{iso} = 0.36 \pm 0.01$ and it was found that this value does not depend on the intensity of the incoming beam. The value of the derivative polarizability was then obtained from Eq. (10) as $r = -0.024 \pm 0.005$. Once the values of R_1, R_2, and R_{iso} were obtained as described above, the order parameters $\langle P_2 \rangle$ and $\langle P_4 \rangle$ were determined from Eqs. (4)–(9). As explained in [32], it is worth noting that the value of R_3 is barely dependent on the thickness of the sample and is practically irrelevant in case that $R_{iso} = 0.2–0.4$. However, it was also measured in order to corroborate Eqs. (5)–(9). Good agreement in the values of R_3 between the experimental and calculated data was found. Finally, the calculated data of $\langle P_2 \rangle$ and $\langle P_4 \rangle$ are presented in Sec. VII D.

B. Order parameters $\langle P_2 \rangle$ and $\langle P_4 \rangle$ determined by PRS, Jones *et al.* method

At the second stage, the Raman intensity profile for two different polarization configurations, I_{zz} and I_{yz}, were studied in the nematic phase as described in Secs. III and IV. However, the Jones method requires also studying the dependence of these profiles on the intensity of the incoming beam. First, the I_{zz} and I_{yz} profiles for the 25 μm sample were recorded under different intensities of the incoming beam. In particular, a change in these profiles is observed when the power of the laser changes from 5 to 2 mW. This behavior is shown in Fig. 7. Second, the I_{zz} and I_{yz} profiles for the 12 and 25 μm samples were obtained using the optical power of 2 mW. The corresponding experimental points are depicted in Fig. 8. It

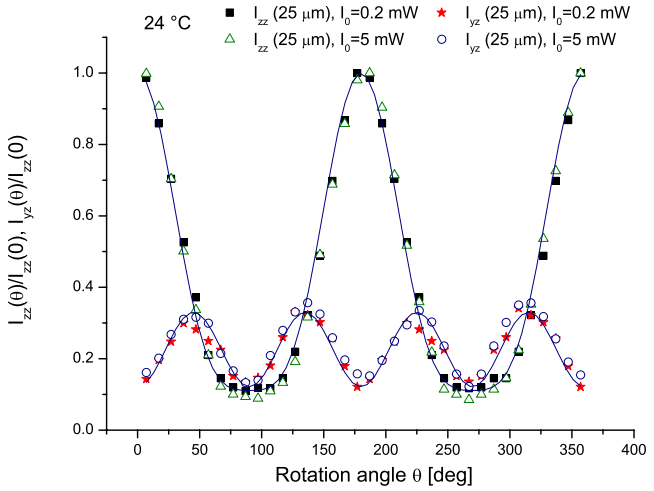

FIG. 7. (Color online) Normalized intensity Raman profiles of the 5CB when the sample is rotated in steps of 10° as described by Jones *et al.* The temperature was held at 24 °C and the 1606 cm^{-1} Raman band was studied. The solid lines are the fitted curves after a χ^2 square procedure according to Eqs. (12) and (13). The dependence of the I_{zz} and I_{yz} profiles on the incoming beam power is illustrated. Although the differences are small, these changes yield slightly different values of $\langle P_2\rangle$, $\langle P_4\rangle$, and r, see Table I.

follows immediately from Figs. 7 and 8 that there is no significant difference for the 12 and 25 μm samples provided the power of the laser is lower than 2 mW. Thus, we have selected these conditions to determine the order parameters following the method developed by Jones *et al.*

The experiments have been undertaken in the nematic phase at temperatures ranging from 34 °C to 24 °C in steps of 2 °C, and a simultaneous fitting procedure of the experimental points in I_{zz} and I_{yz} was carried out using Eqs. (12) and (13). The curves fitted to the experimental points are also shown in Figs. 7 and 8. Using the fitting procedure, the values of $\langle P_2\rangle$, $\langle P_4\rangle$, and r could be determined directly. Apart from that, Table I summarizes the values of $\langle P_2\rangle$, $\langle P_4\rangle$, and r for the 25 μm sample and for two optical powers of the laser in order to get information about the changes in these parameters with respect to a change in the power of the laser. The values of these parameters showed a slight reduction when the power of the laser was kept at 2 mW. In addition, the parameters $\langle P_2\rangle$, $\langle P_4\rangle$ and r were determined at 32 °C for the optical power of 0.02 mW. However, the obtained values of $\langle P_2\rangle=0.42\pm0.02$, $\langle P_4\rangle=0.23\pm0.02$, and $r=-0.18\pm0.01$ are similar to those obtained using the power of 2 mW.

The calculated values of $\langle P_2\rangle$ and $\langle P_4\rangle$, using the laser power of 2 mW, are presented in Sec. VII D.

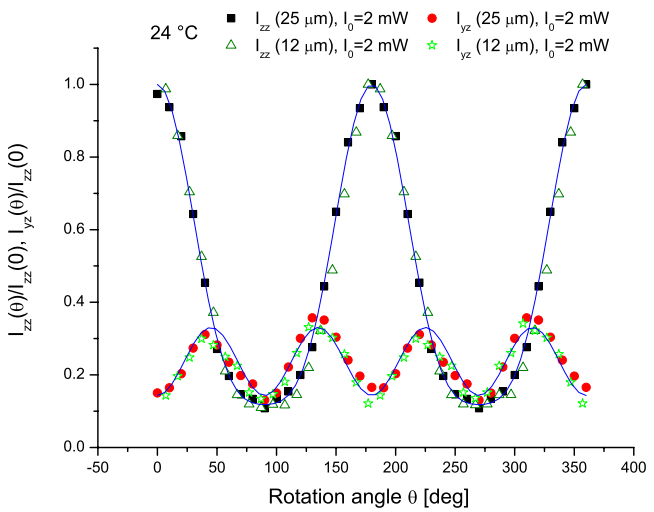

FIG. 8. (Color online) Effect of the sample thickness on the I_{zz} and I_{yz} profiles at 24 °C when the optical power of the laser is 2 mW. The continuous lines are the fitted curves according to Eqs. (12) and (13). The results are practically unaffected by the thickness of the sample if the laser power is low enough.

C. Determining $\langle P_2\rangle$ and $\langle P_4\rangle$ by x-ray scattering

At the third stage, x-ray scattering experiments were carried out in the temperature range from 24 °C to 33 °C with steps of 1 °C. The uniaxial phase was aligned by a magnetic field while the detector recorded the scattered x-ray beam after passing trough the capillary sample. As mentioned in the introduction, an accurate knowledge of the scattered intensity is needed in order to get a good estimation of the order parameters. Davison *et al.* pointed out this inconvenience [28] and proposed a procedure to obtain $I(\chi)$ from the experimental scattered intensity $I_{exp}(\chi)$. The $I_{exp}(\chi)$ from our x-ray data has been corrected following the same procedure and taking the same assumptions. A particular corrected intensity profile $I(\chi)$ integrated around the wide-angle arc χ from the x-ray scattering is shown in Fig. 9. The function $I(\chi)$ is then fitted to Eq. (16) and $\langle P_2\rangle$ and $\langle P_4\rangle$ are directly determined from Eqs. (15) and (17). It is worth noting that the order parameters were also determined following the x-ray method but without using a magnetic field to align the liquid crystal. In this case, the alignment was achieved by the walls of the capillary that contains the liquid crystal. The values of $\langle P_2\rangle$ and $\langle P_4\rangle$ obtained with x-ray were rather similar when the liquid crystal was aligned with either a magnetic field (e.g., for $T=26°$ $\langle P_2\rangle=0.53\pm0.02$ and $\langle P_4\rangle=0.10\pm0.01$) or the walls of the capillary (e.g., for $T=26°$ $\langle P_2\rangle=0.53\pm0.02$ and $\langle P_4\rangle=0.11\pm0.01$). This shows that the order parameters characterize an intrinsic property of the liquid crystal, which is not drastically influenced by changes in the conditions of the x-ray experiment. The assumption of a good oriented phase is therefore satisfied in both cases in order to follow the procedure describe by Davidson *et al.* At the same time, the procedure to correct the $I_{exp}(\chi)$ showed to be accurate enough since the order parameters calculated under both conditions of alignment were almost similar. All the values of $\langle P_2\rangle$ and $\langle P_4\rangle$ determined by x-rays are also depicted in the next section.

D. Orientational order parameters

At the next stage, the experimental values of $\langle P_2\rangle$ and $\langle P_4\rangle$, determined so far, must be compared with the existing theoretical models. The Humphries-James-Luckhurst extends the Maier-Saupe theory assuming a mean field potential of the form $U(\beta)=-A\{\langle P_2\rangle P_2(\cos\beta)+\lambda\langle P_4\rangle P_4(\cos\beta)\}$. The HJL theory therefore couples $\langle P_2\rangle$ and $\langle P_4\rangle$ through the pa-

TABLE I. Values of $\langle P_2 \rangle$, $\langle P_4 \rangle$, and r obtained for different reduced temperatures as well as for two different optical powers of the illuminating laser. The values of $\langle P_2 \rangle$, $\langle P_4 \rangle$, and r have been calculated following the fitting procedure of Jones *et al.* The thickness of the sample is 25 μm.

T_c-T (°C)	Laser power of 5 mW			Laser power of 2 mW		
	$\langle P_2 \rangle$	$\langle P_4 \rangle$	r	$\langle P_2 \rangle$	$\langle P_4 \rangle$	r
10.4	0.60 ± 0.02	0.34 ± 0.01	-0.19 ± 0.01	0.54 ± 0.01	0.30 ± 0.01	-0.16 ± 0.01
8.4	0.55 ± 0.02	0.28 ± 0.01	-0.23 ± 0.01	0.51 ± 0.01	0.30 ± 0.01	-0.15 ± 0.01
6.4	0.57 ± 0.02	0.32 ± 0.01	-0.21 ± 0.01	0.53 ± 0.01	0.25 ± 0.01	-0.18 ± 0.01
4.4	0.52 ± 0.02	0.28 ± 0.01	-0.22 ± 0.01	0.50 ± 0.02	0.26 ± 0.01	-0.19 ± 0.01
2.4	0.45 ± 0.02	0.28 ± 0.01	-0.21 ± 0.01	0.43 ± 0.02	0.23 ± 0.01	-0.17 ± 0.01
0.4	0.38 ± 0.02	0.26 ± 0.01	-0.26 ± 0.02	0.36 ± 0.02	0.22 ± 0.01	-0.21 ± 0.01

rameter λ. The universal MS and HJL theoretical profiles for the two order parameters are shown in Fig. 11 together with the experimental points obtained from the Raman and x-ray measurements. A really good agreement between the results coming from the x-rays analysis and those evaluated using the Jen *et al.* method can readily be seen in Figs. 10. Moreover, the x-ray results are fitted well using the results of the HJL theoretical model and so do the Raman results (Jen *et al.* method). The experimental uncertainty is rather small in those cases, see Fig. 11. In contrast, the $\langle P_4 \rangle$ values evaluated following the Jones *et al.* method are in disagreement with both theoretical models. Although the general tendency of the experimental points is similar to that of the theoretical model, the values are higher than expected. A possible explanation of this behavior is suggested in the following paragraph. Finally, it is worth to emphasize that those two different methods, which probe different features in the molecular system of the uniaxial nematic liquid crystal fitted both to the HJL theoretical prediction.

E. Intensity as a factor in the Raman technique

In the previous section, we have shown that the Raman results are sensitive to the power of the incoming beam when either Jones *et al.* or Jen *et al.* method is used to determine the orientational order parameters. However, the measurements and evaluation using the Jen *et al.* method are clearly insensitive to the intensity of the incoming beam when either a 25 μm sample or an optical power lower than 2 mW is used (see Fig. 5). In contrast, the fitting procedure developed by Jones *et al.* appears to be more sensitive to the changes in the shape of the I_{zz} and I_{yz} profiles, even when these changes are small. This behavior can be seen in Fig. 7 as well as in Table I. Additionally, it was found that the experiments following the Jones *et al.* method yield values of $\langle P_4 \rangle$ higher than those determined by the Jen *et al.* method and beyond the predictions of the mean field theory.

From this point, it should be noted that the evaluation of the order parameters following Jen *et al.* is performed by measuring the Raman scattered signal when the polarization vector of the illuminating beam is parallel or perpendicular to the director (which coincides with the optical axis of the medium). In addition, the generalization, made by Jones *et al.* in order to determine the order parameters, implies measurements when the linear polarization of the incoming beam

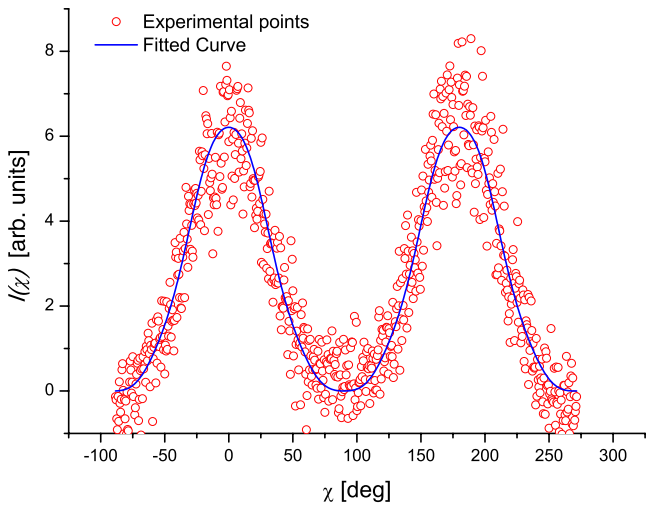

FIG. 9. (Color online) Experimental integrated scattering profile $I(\chi)$ measured in the nematic phase of 5CB at 24 °C. The profile $I(\chi)$ corresponds to the diffraction pattern depicted in Fig. 3. The continuous line represents the fitted curve according to Eq. (16).

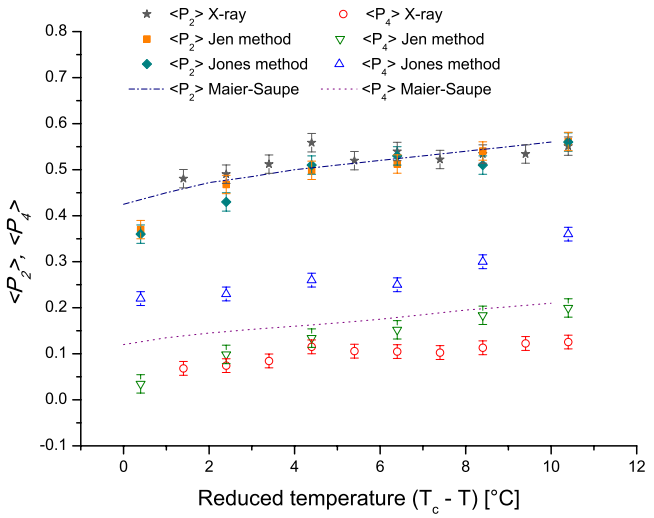

FIG. 10. (Color online) Orientational order parameters $\langle P_2 \rangle$ and $\langle P_4 \rangle$ derived from x-ray measurements and from two different Raman methods for 5CB. The data (points) are compared with the Maier-Saupe theory (dashed lines). Note that the values of $\langle P_4 \rangle$ are always positives.

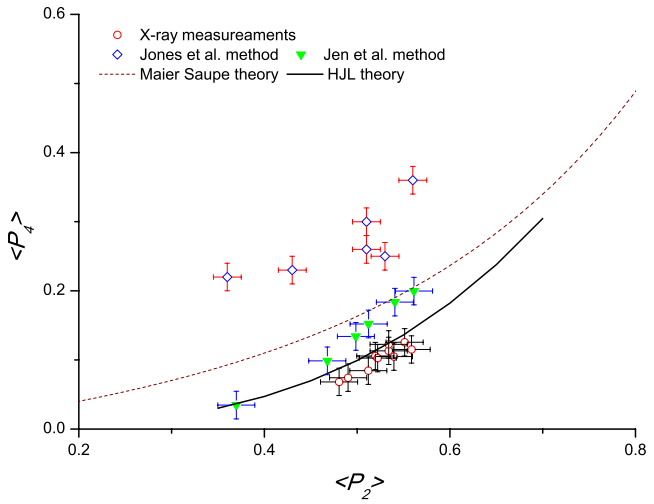

FIG. 11. (Color online) The theoretical curves $\langle P_2\rangle$ vs $\langle P_4\rangle$ predicted by the mean field theories of Maier-Saupe and Humphries-James-Luckhurst are presented ($\lambda=-0.55$, Ref. [5]). The values of $\langle P_2\rangle$ and $\langle P_4\rangle$ determined by PRS and x-ray are compared with the results of these theories.

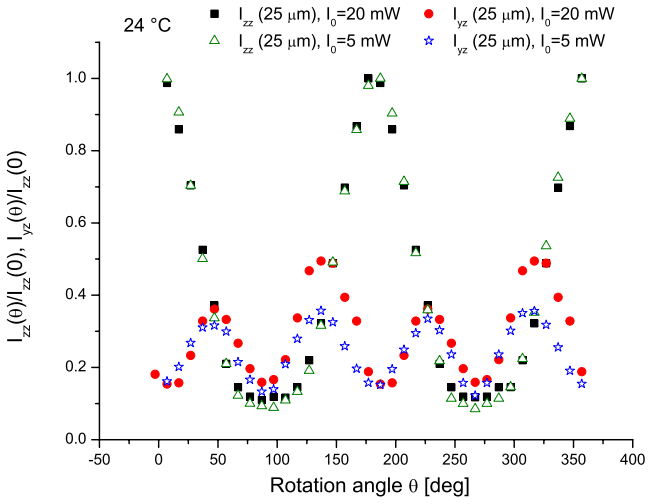

FIG. 12. (Color online) Comparison of the I_{zz} and I_{yz} profiles with two different values of the optical power (from a 25 μm sample). The changes in the I_{yz} profile can readily be seen when the sample is illuminated with the optical power of 20 mW (in a spot of 8 μm in diameter).

makes an angle θ with the optical axis. Under these conditions, the scattered Raman radiation is generated with ordinary o and extraordinary e components. Taking into account that liquid crystals possess a notorious large magnitude of their nonlinear optical susceptibilities [31], a nonlinear process would be possible under the adequate conditions between these o and e waves [33,34]. The dimension of the spot of the focused laser on the sample, using the 50x objective and N.A=0.45, was estimated to be around 8 μm in diameter when the optical laser power of 20 mW was used. A crude estimate of the light intensity in the focused region yields a value of about 4×10^5 W cm^{-2}. This value is high enough to influence the optical response of the material. Thus, under these conditions, the experiment has been carried out to find out if this intensity of light can affect the scattered Raman signal. The corresponding I_{zz} and I_{yz} profiles are depicted in Fig. 12.

It can readily be seen that the I_{yz} profile is drastically influenced by the high intensity of the incoming beam since a clear increase in the scattered Raman signal in the vicinity of the second and fourth peak in this profile is observed. The changes in the I_{zz} profile were actually rather small. This effect could be understood as a stimulated phenomenon where the ordinary and extraordinary waves may interact with each other, which lead to the increase in one of these two components. It should be noted, however, that the interference of ordinary and extraordinary beams is not the only origin of the nonlinear effects. As shown in reference [35], there exists also a nonlinear cubic term in the expression for the molecular dipole induced during the Raman scattering process. This effect has not been taken into account in the derivation of Eqs. (12) and (13) used to evaluate the order parameters. The samples used in those experiments were planar oriented nematic liquid crystals, similarly to our experiments. It is worth to notice that despite the unexpected changes in the I_{zz} and I_{yz} profiles, the ratio of R_1 and R_2 is unaffected. This is not surprising since it was assumed that in order to determine R_1 and R_2, the incoming optical wave must travel along or perpendicular to the optical axis. In this way, a mixing process should be observable only when the polarization vector of the optical field in the sample makes an angle θ with respect to the optical axis different from 0° or 90°.

Additional information is obtained when a 12 μm sample is studied at 32 °C, close to the phase transition into the isotropic phase ($T_c=34.4$ °C), using high intensity of the beam. The results are presented in Fig. 13. In this case, the largest change can be observed in the I_{zz} profile, showing once again that the response of the scattered Raman signal is

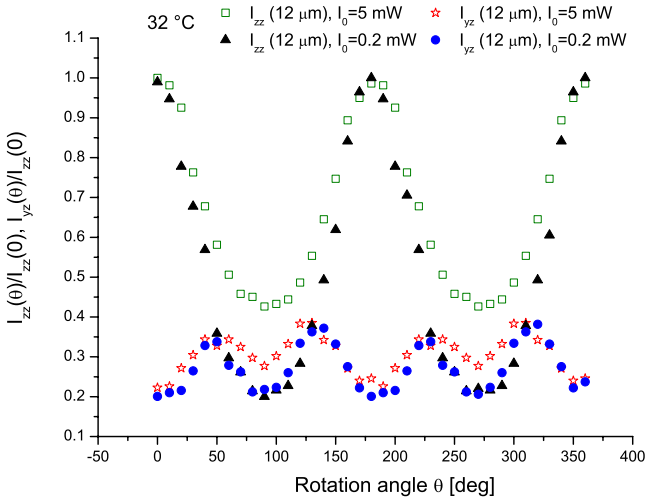

FIG. 13. (Color online) I_{zz} and I_{yz} profiles obtained from the 12 μm sample with two different values of the optical power. The changes are clearly visible in both the I_{zz} and I_{yz} profiles when the sample is illuminated with the optical power of 5 mW (in a spot of 8 μm in diameter). The laser intensity needed to produce significant changes in these profiles is smaller than the corresponding intensity for the 25 μm sample.

significantly affected by the incoming optical field. Hence, it is clear that the response of the Raman signal in either the I_{zz} or I_{yz} profile could be enhanced depending on the experimental conditions. A possible contribution coming from the numerical aperture of the objective is negligible [36,37]. Some influences, however, due to local heating effects from the focused beam cannot be excluded.

Thus, there is an evidence of stimulated Raman scattering in the sample under the experimental conditions of this work and therefore one should be careful measuring these profiles. A more detailed study of the interaction of ordinary and extraordinary waves in the focal region of the sample is required in order to distinguish the physical processes involved in the experiment. Based on these results, one may assume that the I_{zz} and I_{yz} profiles, measured with a laser power lower than 2 mW, are also affected by the optical field. This could lead to mistakes in the evaluation of the order parameters and could hence explain the disagreement in the values of $\langle P_4 \rangle$ obtained using the Jones *et al.* method and the large variations in this parameter found in literature so far.

VIII. CONCLUSIONS

In this paper, we have undertaken the first comparative study of the orientational order parameters $\langle P_2 \rangle$ and $\langle P_4 \rangle$ in a nematic liquid crystal using both x-ray scattering technique and confocal polarized Raman spectroscopy for the same material (5CB). The order parameters have also been determined from Raman spectroscopy data using two different methods proposed by Jen *et al.* [5] and Jones *et al.* [21], respectively. One notes that the advantage of the confocal Raman spectroscopy, used in this study, is the ability to probe small regions of a nematic liquid crystal (of the order of 8 μm in our case) where the incident light is focused. The director orientation in such a small region is always homogeneous, while this is not necessarily the case in much larger regions probed in early studies of nematic liquid crystals using standard Raman setups [5,14].

We have found that the values for $\langle P_2 \rangle$ derived using x-ray scattering and two Raman scattering techniques are in very good agreement with each other. The values of $\langle P_4 \rangle$ determined by using the x-ray scattering technique and the Raman scattering technique proposed by Jen *et al.* are also in good agreement. Moreover, the absolute values and temperature variations in both order parameters are in good agreement with predictions of the Maier-Saupe and HJL mean field theories. At the same time, there is a significant quantitative difference between the values of $\langle P_4 \rangle$ obtained using the methods of Jen *et al.* and Jones *et al.* Nevertheless, the qualitative tendency is the same, and it is important to stress that the values of $\langle P_4 \rangle$, determined by all three methods, are strictly positive throughout the whole nematic phase. Similar to the recent studies, in which polarized Raman spectroscopy has been used [21,22], we never obtained the values of $\langle P_4 \rangle$ lower then those predicted by the HJL theory. This result confirms the results of the previous study [22], and is very much different from the results of the early studies where negative values of $\langle P_4 \rangle$ have been found [14].

In this study, we have also found some quantitative discrepancies concerning the absolute values of $\langle P_4 \rangle$ obtained using two different Raman techniques. Indeed, the values of $\langle P_4 \rangle$ derived from Raman scattering data following the method of Jones *et al.* differ by a factor of 2 from those obtained using the method of Jen *et al.* and the x-ray scattering. As discussed in detail above, this may be related to the effect of the intensity of the incoming beam (which is relatively high in the focused region) on the normalized Raman signal as shown in Figs. 12 and 13. This may stem from various nonlinear optical effects in the liquid crystal medium which have not been taken into account in the derivation of the equations used to determine the order parameters. In particular, the method proposed by Jones *et al.* implies the measurements at various angles θ between the director and the polarization direction of the incoming light wave which generally leads to the birefringence. In a nonlinear regime the ordinary and extraordinary waves may mix yielding an additional contribution to the Raman signal and leading to a change in the dependence of the scattering intensity on the angle θ.

Another nonlinear effect is related to the scattering on individual molecules in the nematic material. As discussed in Ref. [35], in the process of Raman scattering the induced molecular dipole may also contain the nonlinear contribution which is cubic in the amplitude of the local electric field. This contribution may also affect the Raman signal. One notes, that nonlinear effects may, effectively, lead to an apparent temperature variation in some parameters in the general equations used in this paper. Indeed, in the method proposed by Jones *et al.* [21] the differential molecular polarizability r is treated as a free parameter which leads to a very good fitting [22]. This is equivalent to the assumption that the differential molecular polarizability may be temperature dependent and may be different in different phases.

One notes that a possible origin of such an apparent temperature variation may be related to the nonlinear effects. Indeed, in the nonlinear regime the effective differential polarizability contains a contribution which depends on the intensity of the incident light. This contribution is indeed expected to be temperature dependent as it is a function of temperature dependent order parameters in each phase. Thus, a detailed theoretical study of the nonlinear effects associated with Raman scattering in nematic liquid crystals, is required. The corresponding theory will be presented in a separate publication.

ACKNOWLEDGMENT

The first author thanks CONACyT-DAAD for the support.

[1] W. Maier and A. Saupe, Z. Naturforsch. A **15A**, 287 (1960).
[2] P. G. de Gennes and J. Prost, *The Physics of Liquid Crystals*, 2nd ed. (Clarendon Press, Oxford, 1993).
[3] A. J. Leadbetter and E. K. Norris, Mol. Phys. **38**, 669 (1979).
[4] B. Bhattacharjee, S. Paul, and R. Paul, Mol. Phys. **44**, 1391 (1981).
[5] S. Jen, N. A. Clark, and P. S. Pershan, J. Chem. Phys. **66**, 4635 (1977).
[6] I. Chirtoc, M. Chirtoc, C. Glorieux, and J. Thoen, Liq. Cryst. **31**, 229 (2004).
[7] J. W. Emsley, G. R. Luckhurst, and C. P. Stockley, Mol. Phys. **44**, 565 (1981).
[8] M. D. Ossowska-Chruściel, R. Korlacki, A. Kocot, R. Wrzalik, J. Chruściel, and S. Zalewski, Phys. Rev. E **70**, 041705 (2004).
[9] H. Sun, M. D. Roth, and B. M. Fung, Liq. Cryst. **28**, 1469 (2001).
[10] G. R. Luckhurst and R. N. Yeates, J. Chem. Soc., Faraday Trans. 2 **72**, 996 (1976).
[11] S. D. Durbin and Y. R. Sheng, Phys. Rev. A **30**, 1419 (1984).
[12] A. Arcioni, R. Tarroni, and C. Zannoni, Liq. Cryst. **6**, 63 (1989).
[13] R. W. Date, I. W. Hamley, G. R. Luckhurst, J. M. Seddon, and R. M. Richardson, Mol. Phys. **76**, 951 (1992).
[14] K. Miyano, J. Chem. Phys. **69**, 4807 (1978).
[15] S. N. Prasad and S. Venugopalan, J. Chem. Phys. **75**, 3033 (1981).
[16] A. N. Davies, W. J. Jones and A. H. Price, J. Raman Spectrosc., **25**, 521 (1994).
[17] R. Seeliger, H. Haspeklo, and F. Noack, Mol. Phys. **49**, 1039 (1983).
[18] L. G. P. Dalmolen, S. J. Picken, A. F de Jong, and W. H de Jeu, J. Phys. (France) **46**, 1443 (1985).
[19] R. L. Humphries, P. G. James, and G. R. Luckhurst, J. Chem. Soc., Faraday Trans. 2 **68**, 1031 (1972).
[20] S. E. Yakovenko, Zh. Prikl. Spektrosk. **47**, 779 (1987); E. M. Aver'yanov and M. A. Osipov,Sov. Phys. Usp. **33**, 365 (1990).
[21] W. J. Jones, D. K. Thomas, D. W. Thomas, and G. Williams, J. Mol. Struct. **708**, 145 (2004).
[22] C. D. Southern and H. F. Gleeson, Eur. Phys. J. E **24**, 119 (2007).
[23] C. D. Southern, P. D. Brimicombe, S. D. Siemianowski, S. Jaradat, N. Roberts, V. Gortz, J. W. Goodby, and H. F. Gleeson, EPL **82**, 56001 (2008).
[24] F. Giesselmann, R. Germer, and A. Saipa, J. Chem. Phys. **123**, 034906 (2005).
[25] J. P. F. Lagerwall and F. Giesselmann, ChemPhysChem **7**, 20 (2006).
[26] N. Kasai and M. Kakudo, *X-Ray Diffraction by Macromolecules* (Springer, New York, 2005).
[27] M. A. Linne, *Spectroscopic Measurement* (Academic, New York, 2002).
[28] P. Davidson, D. Petermann, and A. M. Levelut, J. Phys. II **5**, 113 (1995).
[29] S. J. Clark, C. J. Adam, H. C. Hsueh, F. Pu, and J. Crain, Mol. Cryst. Liq. Cryst. **302**, 433 (1997).
[30] S. Dhara and N. V. Madhusudana, Eur. Phys. J. E **13**, 401 (2004).
[31] I. C. Khoo, *Liquid Crystals*, 2nd ed, (Wiley, New Jersey, 2007).
[32] L. G. P. Dalmolen and W. H. de Jeu, J. Chem. Phys. **78**, 7353 (1983).
[33] I. C. Khoo, Yu Liang, and H. Li, Opt. Lett. **20**, 130 (1995).
[34] P. Etchegoin and R. T. Phillips, Phys. Rev. E **55**, 5603 (1997).
[35] P. Etchegoin and R. T. Phillips, Phys. Rev. E **54**, 2637 (1996).
[36] G. Turrell, J. Raman Spectrosc., **15**, 103 (1984).
[37] C. Bremard, P. Dhamelincourt, J. Laureyns, and G. Turrell, Appl. Spectrosc. **39**, 1036 (1985).